ACS APPLIED MATERIALS & INTERFACES

Research Article

www.acsami.org

Magnetically Actuated Micropatterns for Switchable Wettability

Dirk-M. Drotlef,[†] Peter Blümler,[‡] Periklis Papadopoulos,[†] and Aránzazu del Campo*,[†]

[†]Max-Planck-Institut für Polymerforschung, Ackermannweg 10, 55128 Mainz, Germany

[‡]Institute of Physics, University Mainz, Staudingerweg 7, 55099 Mainz, Germany

Supporting Information

ABSTRACT: Arrays of actuated magnetic micropillars that can be tilted, twisted, and rotated in the presence of a magnetic field gradient were obtained. The type and extent of the movements are dependent on the distribution (isotropic, anisotropic) of the magnetizable particles inside the pillars and the strength and the direction of the magnetic field gradient. Independent motion of groups of pillars in the same or opposite directions or homogeneous motion of the whole pattern has been realized. Changing the pattern geometry causes changes in the roll-off angle (ROA) of water droplets on the surface. We show magnetically induced changes in the ROA and direction-dependent ROAs as a consequence of the anisotropy of tilted patterns. We also demonstrate transfer of microparticles between magnetically actuated neighboring pillars.

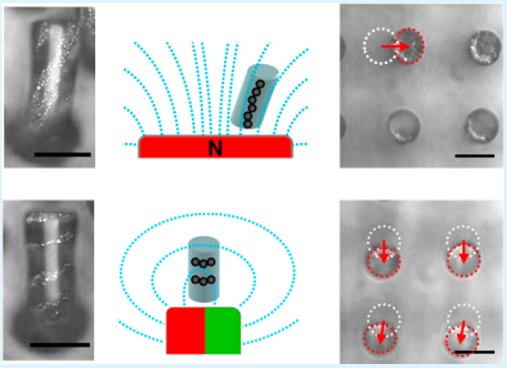

KEYWORDS: *actuated patterns, magnetic responsive polymer, soft actuators, switchable wetting, switchable surfaces, magnetic elastomers*

INTRODUCTION

Topography at the micro- and nanoscale confers distinct properties to materials' surfaces, such as antireflection, enhanced adhesion, a superhydrophobicity or -oleophobicity. Nature provides multiple examples in moth eyes, gecko's attachment pads, and plant leaves. Numerous artificial mimics have been reported with properties and function that closely depend on the geometry and dimensions of the pattern features and change with the surface design.[1,2] Actuated surface topographies with patterned responsive materials allow tuning of surface properties and function on-demand. A few examples have been reported in recent years. Tunable patterned adhesive surfaces (i.e., "gecko" mimics) have been obtained with arrays of micropillars made of shape-memory polymers whose tilting angles with respect to the surface can vary in response to temperature changes[3] or of liquid-crystalline elastomers that exhibit temperature-induced length changes.[4] Tunable wettability based on switchable topographies has been achieved by means of temperature-responsive patterns of liquid-crystalline elastomers[5,6] or mechanically actuated poly(dimethylsiloxane) micropatterns,[7] wrinkles,[8−10] and porous membranes.[11]

Elastomeric materials filled with magnetic nanoparticles and shaped in different microgeometries by soft molding methods undergo predesigned, complex two- and three-dimensional motions upon application of magnetic field gradients.[12−17] This is an attractive strategy for actuation because it does not require sophisticated materials synthesis and the magnetic field selectively addresses magnetic components in the pattern. Magnetic elastomers have been applied in microfluidics,[17] to induce localized traction forces to cells,[13,15] to generate anisotropic motion of microsized objects,[12] and also recently to produce switchable adhesive patterns.[18] Here we demonstrate the possibility of creating different types of individual and collective motion in magnetic micropillar patterns in the presence of magnetic field gradients. Micropillars filled with magnetic nanoparticles tilted, rotated, or made torsional movements depending on the distribution of the nanoparticles inside the pillars (isotropic or anisotropic parallel or perpendicular to the pillar axes) and the spatiotemporal application of magnetic field gradients. We show magnetically switched directional wetting on top of patterned surfaces with changes in the micropillar tilting angle with respect to the surface. We also demonstrate transfer of microparticles between magnetically actuated neighboring pillars. This approach is uncomplicated and flexible, does not require sophisticated material synthesis, and is compatible with any material or surface topographical design.

EXPERIMENTAL SECTION

Materials. Carbonyl iron particles (CIPs) were provided by BASF SE (Ludwigshafen, Germany). They had a spherical shape with an average size distribution between 0.5 and 1 μm (Figure SI-1 in the Supporting Information).

Preparation of the Polydimethylsiloxane (PDMS) Ferrofluid. A 10:1 ratio of Sylgard 184 prepolymer and cross-linker were mixed with CIP microparticles (20 wt %) by stirring manually to get a homogeneous suspension. The mixture was immediately used for molding.

Received: March 13, 2014
Accepted: May 6, 2014
Published: May 6, 2014

   dx.doi.org/10.1021/am5014776 | ACS Appl. Mater. Interfaces 2014, 6, 8702−8707

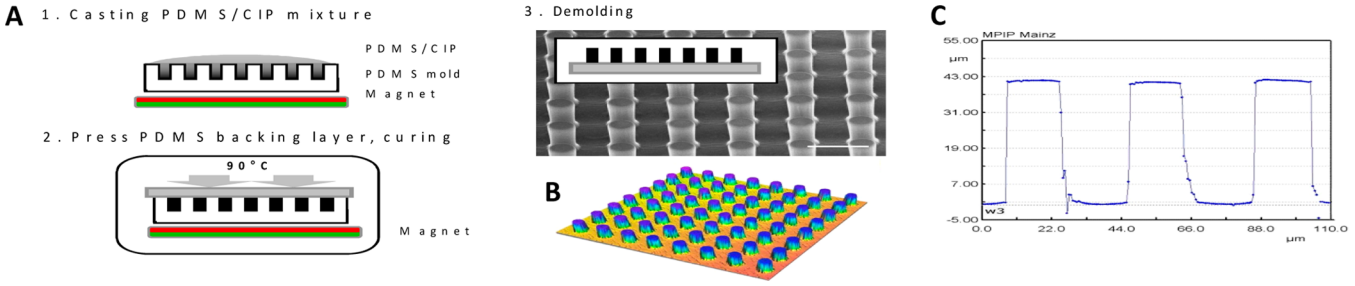

Figure 1. (A) Scheme showing the steps for fabrication of micropillar patterns. The SEM image in step 3 shows the obtained magnetic PDMS pillar pattern. The scale bar corresponds to 40 μm. (B) Confocal microscope picture of magnetic elastomer pattern. (C) Profile of the magnetic elastomer pillars (43 μm height, 18 μm diameter, and 22 μm spacing) as obtained by confocal microscopy.

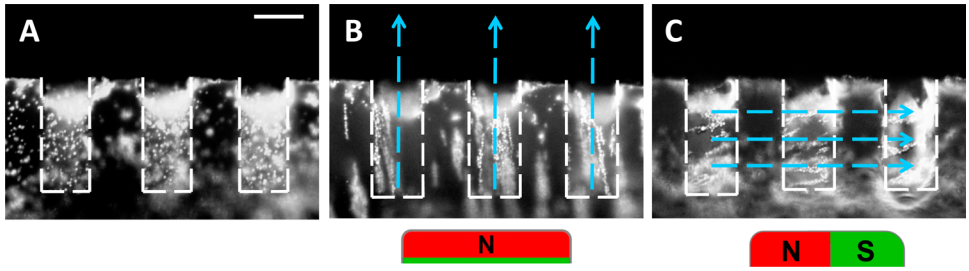

Figure 2. Alignment of microparticles inside the micropillars for different orientations of the magnetic field lines. The microscopic side-view images show the magnetite particles inside the magnetic PDMS in the mold cavities (43 μm depth, 18 μm diameter, and 22 μm spacing) in the presence and absence of a magnet. (A) Randomly distributed particles in the absence of a magnet. (B) Vertically and (C) horizontally aligned particles following the orientation of the magnetic field lines (schematically represented by the light-blue arrows). The scale bar corresponds to 20 μm.

Fabrication of Soft PDMS Molds by Soft Replication. Soft PDMS molds containing holes with a depth of 43 μm, a diameter of 18 μm, and a spacing of 22 μm were obtained by replicating SU-8 lithographic templates with arrays of micropillars with corresponding geometries as previously reported.[19−21] The PDMS molds were treated in an oxygen plasma and exposed to hexadecafluoro-1,1,2,2-tetrahydrooctyltrichlorosilane for 30 min in vacuum and then cured at 95 °C for 30 min. The perfluorinated coating of the PDMS mold was essential to avoid sticking of the mold to the magnetic PDMS in the next replication step.

Preparation of Flat PDMS Backing Layers. Sylgard 184 prepolymer and cross-linker were mixed in a 10:1 ratio, and the mixture was degassed, poured onto a glass Petri dish, and cured for 1 h at 90 °C. The side exposed to the Petri dish was used as the backing of the pillars. The thickness of the film was 1 mm.

Fabrication of Magnetic Micropillar Patterns. The PDMS/CIP mixture was degassed and cast on the PDMS mold. The magnetic particle density in the mold cavities was enhanced by placing the mold on a permanent magnet for 10 min. This was the optimum time for maximum and homogeneous response over the whole pattern field in the later experiments. The magnetic field patterns and response obtained with this protocol were highly reproducible. Longer times did not change the response of the pillars, and shorter times rendered an inhomogeneous response across the patterned field, which we associate with differences in the particle density inside the pattern. The PDMS thin film was pressed against the mold to remove the residual precursor layer, and the sandwich was placed on the magnet again for an additional 10 min. Longer times (30 min) did not improve the final magnetic response of the micropillars any further. The sample was cured at 90 °C for 1 h in a vacuum oven and in the presence of a magnet. Micropatterned PDMS fields with arrays of circular pillars with a height of 43 μm, a diameter of 18 μm, and a spacing of 22 μm were obtained.

Microscopic Setup for Imaging of the Magnetic Response of the Micropillars. The magnetic response of the micropillars was tested by bringing them near a cylindrical NdFeB permanent magnet mounted on a micromanipulator and following their motion by optical microscopy. An alternating magnetic field (from an electromagnet connected to a pulsed generator) was used to switch between the pillars' tilting directions (movie 6 in the Supporting Information).

Attachment of a Microparticle to a Magnetic Micropillar. A silica sphere with a diameter of 10 μm was attached to the tip of a coverslip by means of a micromanipulator and transferred to the magnetic pillar.

ROA Determination. A 10 μL water droplet was applied to the micropatterned PDMS surface using a microsyringe. The sample was fixed to a rotating platform and tilted by a computer-controlled setup (Data Physics, OCA35). The droplet was imaged using a video-microscope. The ROA is the tilting angle just before the droplet rolls off the surface.

RESULTS

1. Preparation of Magnetic Patterns. Arrays of magnetic micropillars with a height of 43 μm, a diameter of 18 μm, and a spacing of 22 μm were obtained by soft molding[19−21] using PDMS precursors containing magnetite microparticles (Figure 1). A drop of magnetic PDMS precursor was placed on the mold, and a magnet was applied in order to accumulate the microparticles inside the pillars (Figure 1, step 1). This step was crucial to obtain a homogeneous and strong magnetic response of the pillars across the pattern. The residual magnetic PDMS layer on the mold was scraped off, and a previously cured PDMS thin film was pressed against the mold (Figure 1, step 2). The PDMS/magnetite−PDMS/PDMS sandwich was placed on a permanent magnet for 10 min. In this step the initially randomly oriented magnetic particles inside the micropillars (Figure 2A) aligned in the direction of the magnetic field lines (Figure 2B,C). When the magnetic field lines were parallel to the long axes of the micropillars (the z direction), the microparticles formed layers aligned with the pillar axes (Figure 2B). When the magnetic field lines were parallel to the surface (the xy plane), the microparticles inside the pillars formed parallel layers perpendicular to the pillar axes

dx.doi.org/10.1021/am5014776 | ACS Appl. Mater. Interfaces 2014, 6, 8702−8707

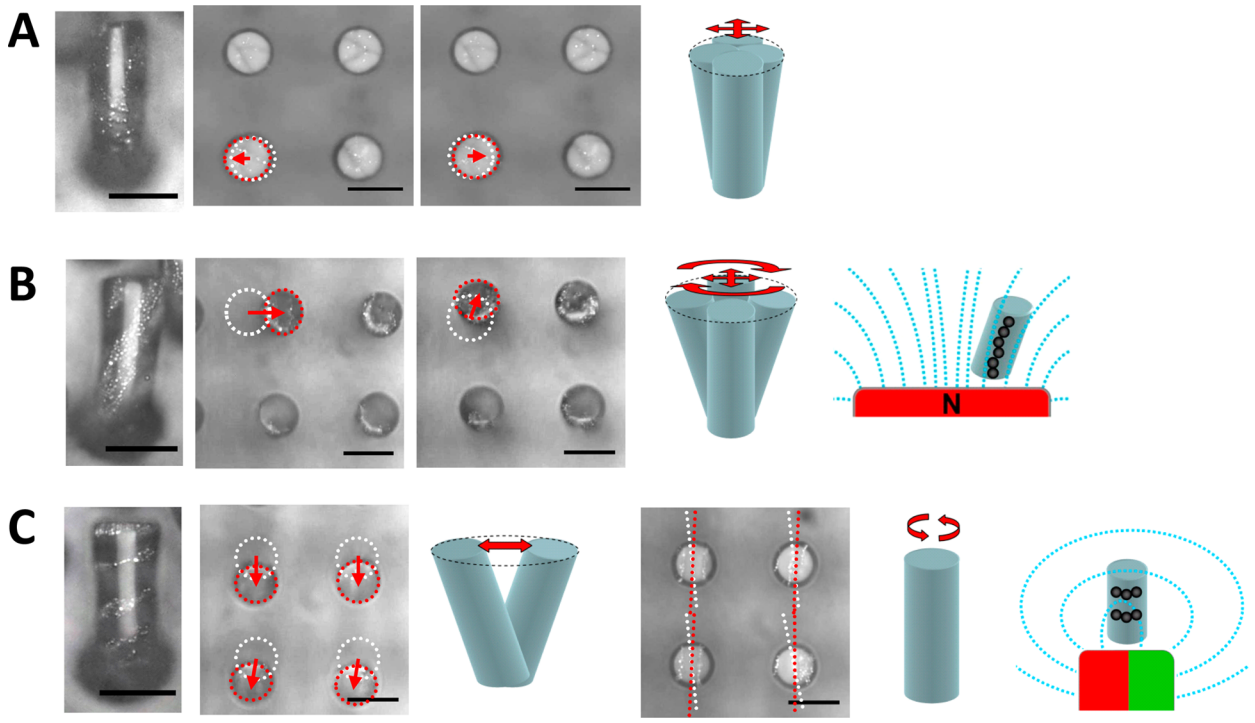

Figure 3. Side- and top-view microscopy images of magnetic pillars containing magnetic particles with different alignments and their movement in the presence of a magnetic field gradient. (A) Pillars with randomly distributed particles showed modest tilting. (B) Pillars with vertically aligned particles bent and rotated about their long axes. (C) Pillars with horizontally oriented particles underwent bending and torsion (twisting) movements. It should be noted that the particle content in (A) is lower than in (B) and (C). Scale bars correspond to 20 μm.

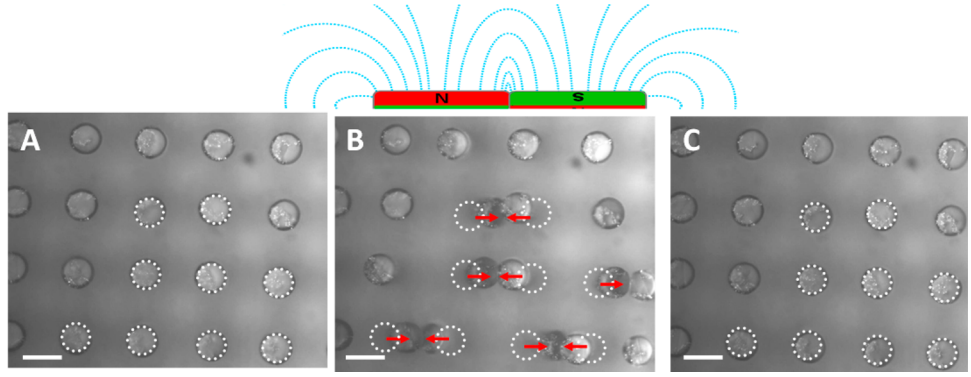

Figure 4. Microscopic pictures showing the movement of micropillars in opposite directions in a steep magnetic gradient caused by two joined magnets (see sketch at the top). A) Pillars in the initial position in the absence of a magnet. B) Tilting of the pillars in opposite directions upon application of a steep magnetic field gradient. C) After removing the magnets, the pillars returned to their initial position. Scale bars correspond to 20 μm. The images correspond to movies 7 and 8.

(Figure 2C and movie 1). In addition to the alignment, the magnetic field also caused an increase in the particle concentration within the pillars versus samples with randomly distributed microparticles. Curing of the PDMS matrix in the presence of the magnet allowed us to freeze the alignment of the magnetic particles within the micropillars. After demolding, homogeneous arrays of magnetic micropillars supported by a PDMS backing layer were obtained.

2. Magnetic Response and Directional Movements. In order to test the magnetic response of the micropillars, a cylindrical NdFeB magnet mounted on a micromanipulator was placed near the sample, and the response of the micropillars was followed by optical microscopy. The response of the pillars was dependent on the applied magnetic field gradient, the direction of the field lines, and the alignment of the microparticles in the pillars. Magnetite–PDMS pillars with randomly distributed microparticles showed a modest tilting angle (1°) when the magnet approached the sample (Figure 3A). Micropillars filled with aligned particles showed stronger movements as a consequence of the higher particle concentration. These movements were maximized when the magnetic field lines were parallel to the particle layers. Micropillars with particles aligned along the pillar axes tilted when the magnet was moved in the *xy* plane (Figure 3B and movie 2) and rotated about their own axes when the magnet was rotated in the *xy* plane (Figure 3B and movie 3). The tilting angle reached 19° at the strongest gradient. When the magnet was removed, the pillars recovered their initial position. Micropillars with particles aligned horizontally (Figure 3C and movies 4 and 5) underwent reversible tilting or twisting

dx.doi.org/10.1021/am5014776 | ACS Appl. Mater. Interfaces 2014, 6, 8702–8707

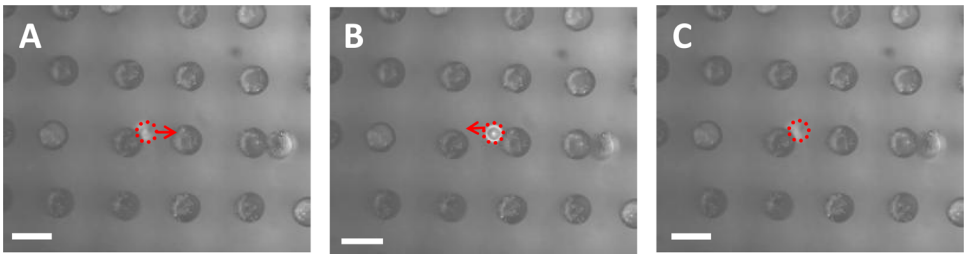

Figure 5. Transfer of a microparticle from one micropillar to the neighboring pillar and back. (A) Pillars in the initial position without the magnet. A silica sphere is attached to the top of a pillar (red circle). (B) The pillars approach each other upon application of two attached magnets as shown in Figure 4, bringing the silica sphere into contact with the other pillar. (C) The sphere was transferred back to the initial position. Scale bars correspond to 20 μm.

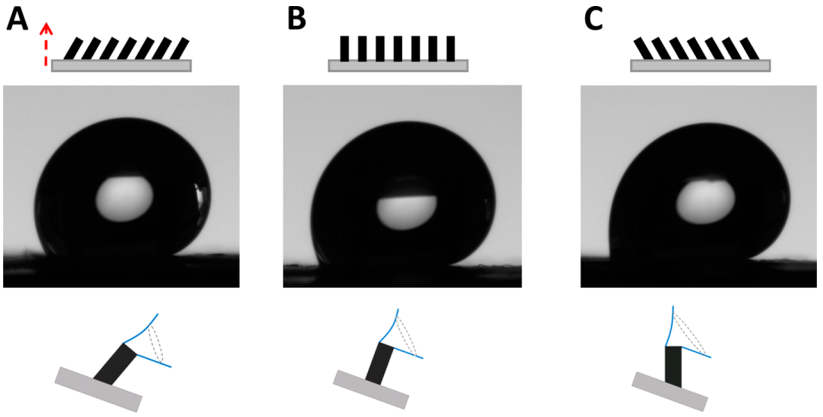

Figure 6. Microscopic images of water droplets deposited on magnetic pillar patterns placed on a tilting stage at the ROA: (A) pillars tilted in the same direction as the tilting stage; (B) pillars in the upright position; (C) pillars tilted in the opposite direction as the tilting stage. Below each image is shown a schematic illustration of the neck formed between the water drop and a single pillar (blue lines). The dotted lines show the variation of the radius of the neck depending on the pillar tilting direction. It should be noted that the narrowest point of the extrapolated form of the neck is inside the pillar.

movements when the magnet was moved or rotated in the *xy* plane, respectively. Homogeneous movement of all pillars was seen within an area of 0.5 cm × 0.5 cm.

Periodic tilting of the micropillars in opposite directions and at variable frequencies was also realized by applying an alternating field using an electromagnet. Tilting angles of 2° were obtained, which are significantly smaller than the values observed with the stronger permanent magnets (movie 6).

Joining two magnets (see the sketch in Figure 4) produced a steep magnetic gradient at the joint, and this was applied to tilt neighboring pillars in opposite directions (Figure 4 and movie 7). With the same arrangement but a less-steep gradient, we were also able to generate a gradient of pillar tilting across the array. Moving the two magnets in a particular direction shifted the tilting of the pillars across the pattern in the selected direction ("*la ola*" in Figure SI-2 and movies 8 and 9).

These results demonstrate the possibility of magnetic actuation of arrays of micropillars, including different types of movements depending on the applied magnetic field and fabrication procedure. In addition, they demonstrate an easy and flexible method to generate changes in the surface topography at the microscale. The next sections demonstrate two examples of applications of magnetically actuated motion: (i) transfer of microparticles at the microscale and (ii) transport of water droplets by magnetically induced topographical and wettability changes.

3. Magnetically Driven Transfer of Microparticles at the Microscale. The movement of micropillars in opposite directions (Figure 4) was used to transfer microparticles from one pillar to the next and back (Figure 5 and movie 10). A 10 μm silica particle was attached to the top of a micropillar using a micromanipulator (Figure 5A). Upon application of the magnetic field, this pillar and its direct neighbor were tilted in opposite directions (as in Figure 4B), and the particle came into contact with both pillars. When the magnetic field was removed, the pillars retracted and the particle was transferred from one pillar to the other (Figure 5B) and back (Figure 5C).

4. Magnetically Induced Wettability Changes. The static, advancing, and receding contact angles (CAs) of the micropillar array were 146°, 160°, and 120°, respectively, when the pillars were in the upright position. As PDMS is inherently hydrophobic, water drops sit on the top of the micropillars, leaving an air layer trapped between the water and the substrate and minimizing the contact area between the water and the solid. This corresponds to a Cassie–Baxter state.[22] When the pillars were tilted by application of a magnetic field gradient, the static CA did not change significantly (145°).

For most applications, the roll-off angle is a more important quantity than the CA. The ROA corresponds to the tilting angle at which the droplet rolls off the surface. The ROA was measured by placing a 10 μL water microdrop on the micropatterned sample and tilting it with the help of a tilting stage. In the absence of a magnet (upright pillars), an ROA of 36° was recorded on the magnetic pillar patterns (Figure 6B). When the magnet was applied and the pillars were tilted 19° in the tilting direction of the stage, the ROA decreased to 26°

dx.doi.org/10.1021/am5014776 | ACS Appl. Mater. Interfaces 2014, 6, 8702–8707

(Figure 6A). When the pillars bent against the tilting direction of the stage, the ROA increased to 46° (Figure 6C). These results demonstrate that magnetically driven changes in the tilting angle of the micropillars can be used to control the ROA of the surface. Moreover, directional ROAs can be achieved as a consequence of the anisotropy of the tilted patterns.

In the following we provide an explanation of these experimental observations based on how wetting occurs at the microscale. The ROA is directly related to the lateral adhesion force between the drop and the substrate. The force holding a tilted drop on a surface (F_s) is directly related to the maximum and minimum CAs along the contour of the drop:

$$\frac{F_s}{\gamma R} = k(\cos\theta_R - \cos\theta_A) \quad (1)$$

where γ is the surface tension of water, θ_R and θ_A are the receding and advancing CAs, respectively, R is the equivalent radius of the drop contour, and k is a dimensionless parameter on the order of 2.0 that depends on the asymmetry of the tilted drop.[23] The receding contact angle (left side of the drop) varies strongly between the upright (120°; Figure 6B) and tilted surfaces. θ_R was 108° on arrays of pillars tilted in the same direction as the tilting direction of the stage (Figure 6A) and 94° on pillars tilted in the opposite direction (Figure 6C). In contrast, the advancing contact angle (right side of the drop) was >160° in all cases. Thus, differences in the ROA can be explained by the differences in θ_R according to the previous equation.

Contact angles of drops on structured surfaces in the Cassie state have been calculated using different approaches. For three-dimensional structures, mainly geometrical arguments have been applied, including the use of average contact angles between solid–liquid and air–liquid interfaces[24] or a modified Cassie–Baxter equation.[25] The approach of Extrand[24] was applied to ratchet nanostructures[26] similar to the ones in this paper. Unlike the case of hairlike posts,[27] the modified Cassie–Baxter equation cannot explain the directional dependence here because the solid–liquid area fraction does not depend on the direction unless partial wetting of the top of the pillars is considered. The model for the ratchet nanostructures yielded good agreement with the experimental values for the receding contact angles in different directions of drop motion. In agreement with our experiments, the easiest roll-off is expected when the pillars and the stage are tilted in the same direction. Here we propose a simple qualitative argument for the directional dependence of the receding contact angle and hence the ROA. On the basis of previous measurements of CAs and lateral adhesion forces on superhydrophobic pillar arrays, which showed that the receding of the water drop occurs by stepwise depinning from single pillars,[28,29] we think that a consideration of surface forces may be more applicable. The receding CA, θ_R, is determined by the capillary force F_c that a single upright or tilted pillar exerts on the water drop at the receding site (Figure 6). Following arguments similar to those in our previous works for drops in the Cassie state,[28] the receding contact angle is given by

$$\gamma d(1 + \cos\theta_R) = F_c \quad \Rightarrow \quad \cos\theta_R = \frac{F_c}{\gamma d} - 1 \quad (2)$$

where γ is the surface tension of water and d is the pillar center-to-center distance. Stronger forces lead to lower receding contact angles and vice versa. As only the top of the pillar is wetted by the drop in a Cassie–Baxter state, a capillary neck forms between the top of the pillar and the nearly spherical drop during receding. The capillary force is roughly $F_c \sim 2\pi r\gamma$, where r is the radius of the neck at its narrowest point. The hydrostatic force at the top surface is neglected here. The neck has a different form depending on the tilting of the pillar, as shown in the sketches in Figure 6. The neck should have approximately the shape of a catenoid, so its narrowest point is not necessarily inside the drop; it may also be inside the pillar after extrapolation of the liquid–air interface. This is always the case in Figure 6. At the advancing site, the orientation of the water–air interface is almost parallel to the substrate, so no net capillary force is exerted. On the receding site, the neck is fixed to the edge of the pillar, and therefore, its orientation with respect to the substrate varies. The neck is thinnest when the pillars are tilted in the same direction as the stage (Figure 6A) and thickest when the pillars are tilted in the opposite direction (Figure 6C). As a consequence, the capillary force from a single pillar and, consequently, the ROA are expected to increase in the order A > B > C, as observed experimentally.

These results demonstrate that magnetically actuated pillar bending can be used to obtain directional wetting of patterned surfaces. Although the observed ROA differences are modest, we predict that the combination of magnetic microstructures with available surface modifications for superhydrophobic surfaces would allow significant improvement in the actuated wetting performance of these surfaces.

CONCLUSIONS

Magnetic micropillars undergo different types of motions under the action of external magnetic field gradients. The reversible changes in the surface topography are followed by significant changes of the macroscopic surface properties. By a reduction in the symmetry of the surface design, directional properties can be achieved. Our data demonstrate this in terms of magnetically switchable wetting and transfer of microparticles. It is important to note that our surface structures were not optimized for these applications. Although the changes observed in these systems were modest, optimized designs including hierarchical or asymmetric features would enable larger property changes. The simplicity of the fabrication procedure and availability of the materials used will allow facile transfer and implementation in technological processes.

ASSOCIATED CONTENT

Supporting Information

SEM image of the magnetic microparticles; microscopy images of tilting propagation through the pattern; movie 1 showing magnetic particles inside the liquid PDMS filling the mold cavities and reorienting with the change in the position of the magnet; movies 2 and 3 showing tilting and rotation of pillars containing microparticles aligned with the pillar axes; movies 4 and 5 showing tilting and torsion movements of pillars containing microparticles aligned perpendicular to the pillar axes; movie 6 showing tilting of the micropillars in two opposite directions at variable frequencies using an electromagnet; movie 7 showing tilting of pillars in opposite directions upon application of a steep magnetic gradient with two joined permanent magnets; movies 8 and 9 showing "*la ola*" tilting of the micropillars across the patterned field; and movie 10 showing transfer of microparticles between neighboring pillars under the action of the magnetic field. This material is available free of charge via the Internet at http://pubs.acs.org.

AUTHOR INFORMATION

Corresponding Author

*E-mail: delcampo@mpip-mainz.mpg.de. Tel: +49 6131 379563.

Notes

The authors declare no competing financial interest.

ACKNOWLEDGMENTS

The authors thank Prof. Manoj Chaudhury (Lehigh University) for helpful discussions. This project was funded by the Deutsche Forschungsgemeinschaft (SPP 1420). D.-M.D. thanks the Max Planck Graduate Center for his Ph.D. grant.

REFERENCES

(1) Boesel, L. F.; Greiner, C.; Arzt, E.; del Campo, A. Gecko-Inspired Surfaces: A Path to Strong and Reversible Dry Adhesives. *Adv. Mater.* **2010**, *22*, 2125−2137.

(2) Yan, Y. Y.; Gao, N.; Barthlott, W. Mimicking Natural Superhydrophobic Surfaces and Grasping the Wetting Process: A Review on Recent Progress in Preparing Superhydrophobic Surfaces. *Adv. Colloid Interface Sci.* **2011**, *169*, 80−105.

(3) Reddy, S.; Arzt, E.; del Campo, A. Bioinspired Surfaces with Switchable Adhesion. *Adv. Mater.* **2007**, *19*, 3833−3837.

(4) Cui, J. X.; Drotlef, D. M.; Larraza, I.; Fernandez-Blazquez, J. P.; Boesel, L. F.; Ohm, C.; Mezger, M.; Zentel, R.; del Campo, A. Bioinspired Actuated Adhesive Patterns of Liquid Crystalline Elastomers. *Adv. Mater.* **2012**, *24*, 4601−4604.

(5) Wu, Z. L.; Wei, R. B.; Buguin, A.; Taulemesse, J.-M.; Le Moigne, N.; Bergeret, A.; Wang, X. G.; Keller, P. Stimuli-Responsive Topological Change of Microstructured Surfaces and the Resultant Variations of Wetting Properties. *ACS Appl. Mater. Interfaces* **2013**, *5*, 7485−7491.

(6) Wu, Z. L.; Buguin, A.; Yang, H.; Taulemesse, J. M.; Le Moigne, N.; Bergeret, A.; Wang, X. G.; Keller, P. Microstructured Nematic Liquid Crystalline Elastomer Surfaces with Switchable Wetting Properties. *Adv. Funct. Mater.* **2013**, *23*, 3070−3076.

(7) Yong, J. L.; Chen, F.; Yang, Q.; Zhang, D. S.; Bian, H.; Du, G. Q.; Si, J. H.; Meng, X. W.; Hou, X. Controllable Adhesive Superhydrophobic Surfaces Based on PDMS Microwell Arrays. *Langmuir* **2013**, *29*, 3274−3279.

(8) Lin, P. C.; Yang, S. Mechanically Switchable Wetting on Wrinkled Elastomers with Dual-Scale Roughness. *Soft Matter* **2009**, *5*, 1011−1018.

(9) Lee, S. G.; Lim, H. S.; Lee, D. Y.; Kwak, D.; Cho, K. Tunable Anisotropic Wettability of Rice Leaf-Like Wavy Surfaces. *Adv. Funct. Mater.* **2013**, *23*, 547−553.

(10) Lee, S. G.; Lee, D. Y.; Lim, H. S.; Lee, D. H.; Lee, S.; Cho, K. Switchable Transparency and Wetting of Elastomeric Smart Windows. *Adv. Mater.* **2010**, *22*, 5013−5017.

(11) Yao, X.; Hu, Y. H.; Grinthal, A.; Wong, T. S.; Mahadevan, L.; Aizenberg, J. Adaptive Fluid-Infused Porous Films with Tunable Transparency and Wettability. *Nat. Mater.* **2013**, *12*, 529−534.

(12) Kim, J.; Chung, S. E.; Choi, S. E.; Lee, H.; Kim, J.; Kwon, S. Programming Magnetic Anisotropy in Polymeric Microactuators. *Nat. Mater.* **2011**, *10*, 747−752.

(13) Sniadecki, N. J.; Anguelouch, A.; Yang, M. T.; Lamb, C. M.; Liu, Z.; Kirschner, S. B.; Liu, Y.; Reich, D. H.; Chen, C. S. Magnetic Microposts as an Approach To Apply Forces to Living Cells. *Proc. Natl. Acad. Sci. U.S.A.* **2007**, *104*, 14553−14558.

(14) Glazer, P. J.; Leuven, J.; An, H.; Lemay, S. G.; Mendes, E. Multi-Stimuli Responsive Hydrogel Cilia. *Adv. Funct. Mater.* **2013**, *23*, 2964−2970.

(15) Khademolhosseini, F.; Chiao, M. Fabrication and Patterning of Magnetic Polymer Micropillar Structures Using a Dry-Nanoparticle Embedding Technique. *J. Microelectromech. Syst.* **2013**, *22*, 131−139.

(16) Sniadecki, N. J.; Lamb, C. M.; Liu, Y.; Chen, C. S.; Reich, D. H. Magnetic Microposts for Mechanical Stimulation of Biological Cells: Fabrication, Characterization, and Analysis. *Rev. Sci. Instrum.* **2008**, *79*, No. 044302.

(17) Fahrni, F.; Prins, M. W. J.; van IJzendoorn, L. J. Micro-Fluidic Actuation Using Magnetic Artificial Cilia. *Lab Chip* **2009**, *9*, 3413−3421.

(18) Drotlef, D. M.; Blümler, P.; del Campo, A. Magnetically Actuated Patterns for Bioinspired Reversible Adhesion (Dry and Wet). *Adv. Mater.* **2014**, *26*, 775−779.

(19) del Campo, A.; Greiner, C.; Alvarez, I.; Arzt, E. Patterned Surfaces with Pillars with Controlled 3D Tip Geometry Mimicking Bioattachment Devices. *Adv. Mater.* **2007**, *19*, 1973−1977.

(20) del Campo, A.; Greiner, C.; Arzt, E. Contact Shape Controls Adhesion of Bioinspired Fibrillar Surfaces. *Langmuir* **2007**, *23*, 10235−10243.

(21) Greiner, C.; del Campo, A.; Arzt, E. Adhesion of Bioinspired Micropatterned Surfaces: Effects of Pillar Radius, Aspect Ratio, and Preload. *Langmuir* **2007**, *23*, 3495−3502.

(22) Cassie, A. B. D.; Baxter, S. Wettability of Porous Surfaces. *Trans. Faraday Soc.* **1944**, *40*, 546−550.

(23) ElSherbini, A.; Jacobi, A. Retention Forces and Contact Angles for Critical Liquid Drops on Non-Horizontal Surfaces. *J. Colloid Interface Sci.* **2006**, *299*, 841−849.

(24) Extrand, C. W. Model for Contact Angles and Hysteresis on Rough and Ultraphobic Surfaces. *Langmuir* **2002**, *18*, 7991−7999.

(25) Choi, W.; Tuteja, A.; Mabry, J. M.; Cohen, R. E.; McKinley, G. H. A Modified Cassie−Baxter Relationship To Explain Contact Angle Hysteresis and Anisotropy on Non-Wetting Textured Surfaces. *J. Colloid Interface Sci.* **2009**, *339*, 208−216.

(26) Malvadkar, N. A.; Hancock, M. J.; Sekeroglu, K.; Dressick, W. J.; Demirel, M. C. An Engineered Anisotropic Nanofilm with Unidirectional Wetting Properties. *Nat. Mater.* **2010**, *9*, 1023−1028.

(27) Barahman, M.; Lyons, A. M. Ratchetlike Slip Angle Anisotropy on Printed Superhydrophobic Surfaces. *Langmuir* **2011**, *27*, 9902−9909.

(28) Papadopoulos, P.; Mammen, L.; Deng, X.; Vollmer, D.; Butt, H. J. How Superhydrophobicity Breaks Down. *Proc. Natl. Acad. Sci. U.S.A.* **2013**, *110*, 3254−3258.

(29) Pilat, D. W.; Papadopoulos, P.; Schaffel, D.; Vollmer, D.; Berger, R.; Butt, H. J. Dynamic Measurement of the Force Required To Move a Liquid Drop on a Solid Surface. *Langmuir* **2012**, *28*, 16812−16820.